

Strength Degradation of Thermally Tempered Glass Plates

D. B. MARSHALL and B. R. LAWN

Department of Applied Physics, School of Physics, University of New South Wales, Kensington, N.S.W. 2033, Australia

An earlier theory of contact-induced strength degradation of brittle materials is extended to include plates in residual surface compression. The scale of the strength-controlling flaw is predicted by indentation fracture mechanics, with the modifying effect of the residual field incorporated into both indentation and strength equations. Experimental verification of the predictions is obtained from diamond-pyramid indentation tests on thermally tempered glass plates. As with untempered plates, the theory accounts for the load dependence of the strength loss; it also explains the insensitivity of the degradation characteristics to initial flaw distribution and identifies toughness as the controlling material parameter. Most significant, however, is the demonstration that surface strengthening can produce dramatic improvements in degradation resistance. The possibility of obtaining all parameters necessary for a complete degradation analysis of a given tempered material entirely by routine indentation/strength testing is discussed.

I. Introduction

WHEN plates of glass or other ceramic material are exposed to any environment containing small, hard particles, severe strength losses may result from contact-induced microfracture.¹ Previous papers on this subject²⁻⁴ have established a rationale, based on model blunt/sharp, static/impact indentation systems, for

investigating the seemingly complex and diverse mechanisms of degradation. Basically, for a given indenter/specimen system where the prospective contact surface is free of preexisting stress, up to three regions of strength response may be distinguished according to contact load (or velocity): at low loads, the contact is not severe enough to produce a "dominant flaw," and the strength remains controlled by the prior flaw distribution on the specimen surface; at intermediate loads, the size of the indentation crack begins to exceed the size of preexistent flaws (although in going from sharp to blunt indenters this transition can be greatly suppressed by an increased crack-formation threshold), beyond which the strength decreases; at high loads, the well-developed indentation crack grows stably in penny-like fashion⁵ (regardless of whether the indenter be blunt or sharp), and the strength declines steadily. The indentation fracture approach to the degradation problem provides explicit expressions for the strength over the entire load range, giving a sound basis for optimization of material parameters in structural design.

A question currently receiving increased attention in the general field of ceramic strength is especially relevant to the topic of degradation⁶: for a given materials system, how may the exposed surfaces be strengthened? Removing flaws (e.g. by etching) is of little or no use, since any single subsequent contact event can initiate

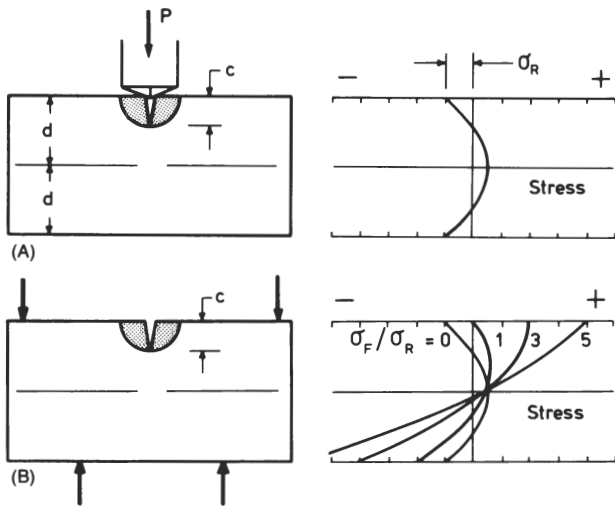


Fig. 1. Schematic of indentation-induced strength degradation. (A) Initial contact event, in which well-developed penny-like cracks (shaded area) achieve stable equilibrium in composite $P + \sigma_R$ field. (B) Subsequent tensile loading (flexure), in which remnant cracks achieve unstable equilibrium in composite $\sigma_F + \sigma_R$ field.

its own flaws,^{2,3} especially with high loads and sharp indenters. The most practical approach to strengthening is to introduce a state of residual compression into the surfaces. Such compression imposes a net closure force on all existing surface flaws, and would be expected to inhibit the initial extension of any indentation-induced cracks, thereby improving resistance to degradation in two ways. There are various ways of achieving this type of strengthening, but all may be classified as either physical or chemical tempering. Silicate glasses have been successfully subjected to tempering processes for many years, but applications to polycrystalline ceramics are only recent.⁷

Prerequisite to a proper understanding of surface degradation in strengthened materials is information on the role of residual stresses in the mechanics of indentation fracture. Such information is given in a detailed theoretical analysis of contact-induced failure of tempered plates by the present writers.⁸ In that study, the cracks were shown to be inhibited in their initial growth through the near-surface region of high compression and conversely enhanced (toward instability) in their subsequent growth toward the inner region of high (counterbalancing) tension in the plate. Where the indentation event leaves a remnant crack without itself causing plate failure, the theoretical analysis may be readily adapted, with minor simplifications, to quantitative predictions of strength-loss characteristics.

It is the aim of the present work to demonstrate the application of indentation-fracture principles to surface-strengthened systems, with minimum complication. Accordingly, only static loading is considered, any differences between this and impact loading (except at near-sonic velocities) being secondary in the degradation behavior.⁴ Also, attention is focused on sharp indenters, since these are associated with maximum severity in fracture damage,³ and thence conservative design. Silicate glass, which is easily tempered and has numerous other advantages as a model brittle solid,²⁻⁴ is selected as a test material. The study is confined to thermally tempered plates because of their relatively simple and slowly varying residual-stress profile.⁸ The choice of a particular system for detailed investigation therefore introduces several simplifying features into the description; however, this is not to imply loss of generality in the basic approach. The present work shows that surface strengthening can lead to substantial improvements in degradation resistance.

II. Prediction of Strength Degradation Characteristics

As in the previous procedure²⁻⁴ the degradation problem is treated in 2 parts (Fig. 1(A), (B)). In (A), an explicit relation between characteristic crack size, c , and indentation load, P , is

sought. Here the indentation fracture mechanics must incorporate the effect of the residual-stress field. In (B), a starting equation for the strength, σ , in subsequent plate flexure, is written in terms of c . The 2 results are then combined to obtain a characteristic degradation function $\sigma(P)$. Again, the strength equation must allow for residual-stress terms. For thermally tempered plate the residual-stress profile across the plate section is closely parabolic, ideally with the outer compression σ_R twice the inner tension; the corresponding profile of flexural stresses is linear, with a maximum σ_F in tension and compression on opposite surfaces.⁹ In any of the configurations in Fig. 1 the effects of stress variations over the prospective crack area may be regarded as small in the fracture mechanics if $c \ll d$, d being the plate half-thickness.

In the subsequent formulation the dependent variables (σ or c) for prescribed indenter-loading and residual-stress conditions will be superscripted by T (tempered) and O (untempered).

(1) Indentation Fracture Mechanics

In determining an appropriate indentation fracture function $c(P)$, it is assumed that the thermal tempering process does not affect the fracture mechanics parameters of the test material.* Crack growth may then be considered in terms of a linear superposition of the indentation and residual-stress fields. For the present it is sufficient to summarize only essential results of previous analyses along these lines.

First, the fracture configuration in the absence of the residual field is considered. In their well-developed form all indentation cracks extend on a near-circular front, provided they are not large enough to "see" the far surface of the plate (i.e. $c \ll d$); they are governed by the simple relation⁵

$$P/c^{3/2} = K_c/\chi = \text{constant} \quad (1a)$$

where $K_c = [2\Gamma E/(1-\nu^2)]^{1/2}$ is the critical stress-intensity factor for equilibrium extension in the test material (with Γ the fracture-surface energy, E Young's modulus, ν Poisson's ratio), and χ is a dimensionless indenter constant (which depends on indenter shape, etc.). Before they achieve this penny-like configuration the cracks must overcome some energy barrier as they pass through a complex formation stage. However, for sharp indenters on glass, where deformation processes in the region of the hardness impression control the formation of downward-extending cracks on median planes (Fig. 1), the scale of the fracture at "pop-in" is hardly sufficient to provide a dominant flaw; in such a case there is no manifestation of a critical indentation load in the degradation characteristics.³ Even in those materials where a threshold is apparent, ignoring it (in applying Eq. (1a)) simply causes an overestimation of true crack size, and thus, ultimately, a conservative strength prediction.

Next, the residual field is introduced into the fracture mechanics. Equation (1a) then modifies to^{8,13}

$$P/c^{3/2} = (K_c/\chi)[1 + \sigma_R(\pi\Omega c^T)^{1/2}/K_c] \quad (1b)$$

where Ω is a dimensionless crack-geometry term. If the small-scale fracture condition $c \ll d$ remains satisfied the residual compressive stress across the crack area is effectively uniform at σ_R . In this approximation the penny-like configuration is retained; analysis then gives $\Omega \approx 4/\pi^2$.⁸ Constant Ω in Eq. (1b) implies stable crack growth (i.e. $dP/dc^T > 0$); however, because of the approach to instability for large-scale extension toward the central regions of the plate,⁸ Ω must ultimately become a diminishing function of crack size (see Sect. IV).

(2) Strength Equations

The standard equation for the tensile strength of a brittle plate in its normal, untempered state, at equilibrium ($\sigma = \sigma_F$, $K = K_c$), is

*The material parameters which may be expected to enter the fracture mechanics are stiffness and toughness, and perhaps hardness. Since thermal tempering is a rapid process (≈ 10 s), compositional changes across the plate section are likely to be negligible; this leaves the residual strains as the major potential source of influence. Stiffness is indeed strain dependent in glasses (Ref. 10), but the maximum residual strain attainable in thermally tempered plate is always < 0.01 , well within the range of linear elastic behavior. Toughness is independent of strain state in brittle solids, since fracture energies are defined in terms of a reversible separation process in which both initial and final states are free of any extraneous forces (Ref. 11). Hardness is found empirically to be similar on tempered and untempered glass surfaces (Ref. 12).

$$\sigma^0 = [2\Gamma E / \pi(1 - \nu^2)c_f^0]^{1/2} = K_c / (\pi c_f^0)^{1/2} \quad (2a)$$

where c_f refers to the dominant flaw, being the "effective length" of an "equivalent through crack." For a tempered plate, using the principle of linear superposition of stress fields, a simple modified version of Eq. (2a) may be obtained¹⁴:

$$\sigma^T = K_c / (\pi c_f^T)^{1/2} + \sigma_R \quad (2b)$$

The source of the dominant flaw in an indented surface will then depend on whether the size of the median cracks exceeds the size of preexisting flaws: at low loads, $P < P'$ (say), the original flaws dominate, and the effective length remains independent of load at some characteristic value, e.g. c_{f0} ; at high loads, $P > P'$, the indentation cracks dominate, and the effective length increases with load (Eq. (1)). Then, without distinguishing between tempered and untempered states,

$$c_f = c_{f0} \quad (P < P') \quad (3a)$$

$$c_f = \Omega c \quad (P > P') \quad (3b)$$

Recall that $\Omega \approx 4/\pi^2$ in the approximation of small-scale cracking.

Ideally, it would be an advantage to obtain an explicit degradation function $\sigma(P)$ from Eqs. (1) to (3). However, because Eq. (1b) is quartic in c^T , the analytic solutions at high load ($P > P'$) are implicit in σ^T :

$$\sigma^T = K_c / (\pi c_{f0})^{1/2} + \sigma_R \quad (P < P') \quad (4a)$$

$$P = [K_c^4 / \chi(\pi\Omega)^{3/2}] [(\sigma^T / (\sigma^T - \sigma_R))^4] \quad (P > P') \quad (4b)$$

Alternatively, crack size may be retained as a parametric variable and Eqs. (1) to (3) solved simultaneously by numerical means.

A useful quantity which highlights the factors contributing to the increase in degradation resistance resulting from tempering is obtained by subtracting Eqs. (2a) and (2b) at constant load:

$$\sigma^T - \sigma^0 = K_c [(1/\pi c_f^T)^{1/2} - (1/\pi c_f^0)^{1/2}] + \sigma_R \quad (5)$$

In this quantity, which may be called the strengthening, the first term on the right-hand side represents the effect due to the diminished crack size in the indentation process, and the second term represents the closure effect on the crack in the subsequent flexure test.

III. Experimental Procedure and Results

(1) Indentation/Strength Test Procedure

Optical quality crown glass lenses (50 mm in diam. and 3 mm thick) were used as test specimens. These were chosen because they are commercially available in the thermally tempered state, and because they have special advantages in strength testing. With these specimens a complete range of surface compression values, from a maximum in the as-received state to zero, was readily obtained by controlled annealing.¹⁵ The stress values were measured by applying Eq. (1b) in the indentation tests,¹³ recording the crack size at specified indentation load, and using calibration values for K_c and χ (Section III(2)) along with the small-scale cracking approximation for Ω . Conventional optical birefringence techniques, using a variable compensator,¹⁶ provided a consistency check, but, since they required an extrapolation of an averaged center stress measurement for a given plate, they gave less reliable indication of σ_R . Appendix A gives a more detailed account of the residual stress measurements.

A standard Vickers diamond pyramid was used to introduce the indentation cracks into the specimen surfaces. A microhardness testing machine* delivered loads within 10^{-1} to 10^2 N, and a universal testing machine† within 10^1 to 10^3 N. Each contact event lasted typically 10 to 20 s. Each lens was indented several times at a prescribed load within a central test area of ≈ 2.5 mm radius, to lessen the possibility of underestimating the degradation. Most specimens were indented with their surfaces in the as-received mechanical state; however, with a few fully tempered surfaces the

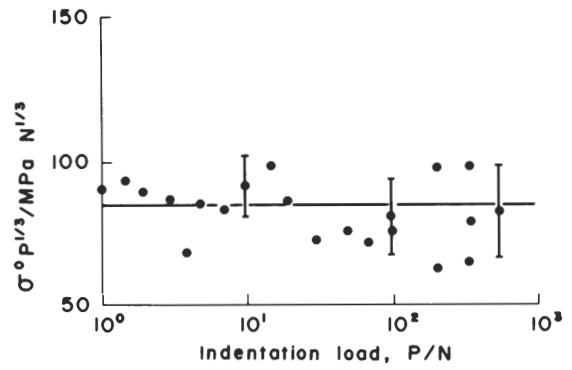


Fig. 2. Indentation/strength data for Vickers diamond pyramid on as-received annealed glass surfaces. Data points with error bars represent mean and standard deviation of ≥ 10 tests at given P ; horizontal line is best fit to data.

prospective test area was prebraded with 320 mesh SiC grit, to introduce a controlled density of flaws, or preetched, to remove preexisting flaws. In all cases the test area was covered with a drop of paraffin oil immediately after preparation to minimize moisture-assisted kinetic effects in the subsequent indentation processes. The damage morphology was essentially the same for all degrees of tempering, other than a diminished scale of cracking relative to the hardness impression with higher surface compression.^{13,17}

For the strength tests, the lenses were mounted in a center-symmetrical bending jig,¹⁸ indented face in tension, and loaded to failure. The failure time was typically 10 to 20 s. This arrangement has two main advantages over the 4-point bend test used in the previous studies²⁻⁴: (1) the applied stress is essentially uniformly biaxial, as is the residual stress field, so that all median cracks experience maximum normal loading regardless of orientation; (2) premature edge failures are excluded, although failures at the support rings are not (instances of support failures were rare, however, and were rejected from the data accumulation). The strength was evaluated from the formula

$$\sigma_F = kQ/d^2 \quad (6)$$

where $\sigma = \sigma_F$ corresponds to a critical flexure load Q . For the constant in this equation, Wilshaw¹⁸ gives $k = (3/8\pi)[(1 - \nu)(b^2 - a^2)/2r^2 + (1 + \nu) \ln(b/a)]$; in the present tests, $a = 8.0$ mm was the inner support radius, $b = 19.8$ mm the outer support radius, $r = 25$ mm the lens radius, and $\nu = 0.25$ the Poisson's ratio for glass, giving $k = 0.158$.

The total time span between specimen preparation (if any), indentation, and strength testing, never exceeded 4 h.

(2) Annealed Plates: Determination of Fracture Mechanics Parameters

The constants K_c and χ must be determined before Eq. (4) can be used to make *a priori* strength predictions for tempered plates, and Eq. (1b) can be used to determine appropriate σ_R values. These constants were obtained from 2 sets of calibration tests on fully annealed plates.

The first tests were made using a standard diamond pyramid indentation procedure, in which crack sizes, as measured in terms of median surface traces along the impression diagonals,^{5,19} were recorded as a function of load. These tests were conducted in a dry nitrogen atmosphere, to ensure near-equilibrium conditions. Inserting the results into Eq. (1) gives $K_c/\chi = P/c^0^{3/2} = (8.2 \pm 0.4)$ MPa $m^{1/2}$ (mean \pm standard deviation, ≈ 100 indentations over load range 10^0 to 10^2 N).

The second set of tests was made with a preliminary indentation/strength run on ≈ 50 as-received, fully annealed lenses. For the special case $\sigma_R = 0$, Eq. (4b) in the region where the indentation crack provides the dominant flaw reduces to an explicit $\sigma(P)$ function:

$$\sigma^0 P^{1/3} = (K_c^4/\chi)^{1/3}/(\pi\Omega)^{1/2} = \text{constant} \quad (P > P') \quad (7)$$

A best-fit to the data in Fig. 2 gives $(K_c^4/\chi)^{1/3}/(\pi\Omega)^{1/2} = (84 \pm 12)$ MPa $N^{1/3}$.

*Zwick, Testing Machines Inc., Amityville, N.Y.
†Instron Corp., Canton, Mass.

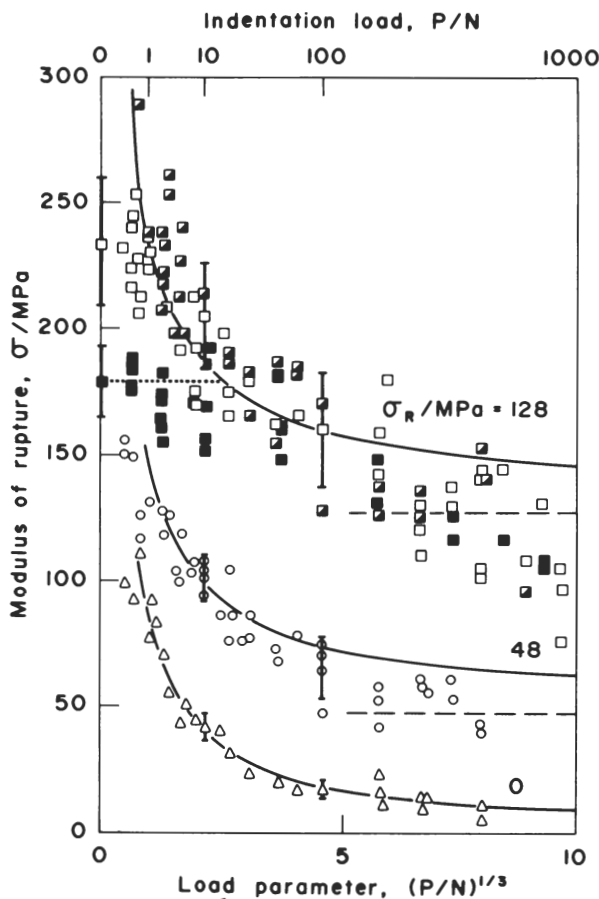


Fig. 3. Strength of glass surfaces as a function of Vickers indentation load, for 3 tempering states. *Open symbols* designate as-received surfaces, *filled symbols* preabraded surfaces, and *half-filled symbols* pre-etched surfaces; data points with error bars represent mean and standard deviation of ≥ 10 tests at given P . *Solid curves* are predictions from Eq. (4) at $P > P'$; *dotted horizontal line* is a fit to data for preabraded surfaces at $P < P'$; *broken lines* are asymptotic predictions at $\sigma = \sigma_R$.

The 2 required constants may now be uniquely determined from the above 2 calibration equations: with $\Omega = 4/\pi^2$, $K_c = (0.47 \pm 0.07) \text{MPa m}^{1/2}$ and $\chi = 0.057 \pm 0.011$. An independent measure of the critical stress-intensity factor using the double-cantilever arrangement²⁰ (by Wiederhorn) gave $K_{Ic} = (0.78 \pm 0.13) \text{MPa m}^{1/2}$ (mean \pm standard deviation, 6 specimens). The relatively low value of K_c from the indentation/strength tests is presumed to reflect the omission from the fracture mechanics of residual-stress effects about the elastic/plastic impression,^{21,22} but is nevertheless preferred since the remainder of the indentation/strength experiments were conducted under identical conditions. Appendix B gives an elaboration of the residual-stress effects in the present context.

(3) Tempered Plates: Effect of Indentation Load on Degradation

The most extensive series of tests investigated the effect of indentation load on strength loss, at a specified degree of tempering, i.e. $[\sigma(P)]_{\sigma_R}$. Data were taken for 3 tempering states: fully tempered, $\sigma_R = (128 \pm 15) \text{MPa}$; partially tempered, $\sigma_R = (48 \pm 5) \text{MPa}$; and fully annealed, $\sigma_R = (0 \pm 2) \text{MPa}$ (all values mean \pm standard deviation, 8 lenses), with different specimen surface preparations (Section III(1)). Figure 3 shows the results, with experiment represented by the data points and theoretical prediction from Eq. (4b) in the indentation-controlled region represented by the full curves. The relatively large scatter in data for the more highly tempered plates was attributed to slight (reversible) warpage in the plates during tempering, resulting in a distortion of the ideally uniform, biaxial stress field in the center-symmetrical bend test. Allowing for this

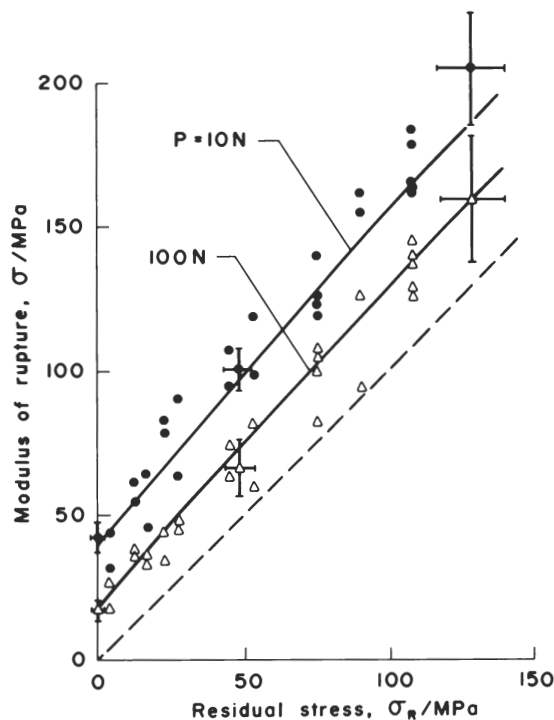


Fig. 4. Strength of as-received glass surfaces as a function of residual compressive stress, for 2 Vickers indentation loads. Data points with error bars represent mean and standard deviation of ≥ 10 tests at given σ_R . *Solid curves* are predictions from Eq. (4) at $P > P'$; *broken line* at $\sigma = \sigma_R$ is lower limit of strength (Eq. (2b)).

scatter, the predicted and observed results agree reasonably over the greater part of the load range covered.

The general trends in Fig. 3 highlight the strengthening effect of the tempering process. Toward high loads the strength curves for each degree of tempering decline gradually, independently of initial surface preparation, tending asymptotically (with some overshoot) as $\sigma \rightarrow \sigma_R$. Toward low loads the curves rise more steeply, cutting off at some level characteristic of the surface condition: for abraded surfaces, with their uniform density of flaws, the cutoff is reasonably well-defined; for etched surfaces, presumably with all of the severe preexisting flaws removed, there is no evidence of cutoff within the strength range examined; for as-received surfaces, the data tend to scatter between these 2 extremes.

(4) Tempered Plates: Effect of Surface Compressive Stress on Degradation

Another series of tests investigated the effect of degree of tempering on strength characteristics, at specified contact conditions, in greater detail, i.e. $[\sigma(\sigma_R)]_P$. Data were collected at 2 fixed loads, $P = 10 \text{ N}$ approaching the low-load region and $P = 100 \text{ N}$ approaching the high-load region, on as-received surfaces. These data, along with the degradation curves evaluated from Eq. (4), are plotted in Fig. 4; the dramatic increase in resistance to degradation with degree of tempering is again evident, along with the relatively innocuous effect of indentation load.

IV. Discussion

As in previous studies,²⁻⁴ a simplistic indentation/strength analysis provides an adequate basis for predicting strength degradation characteristics. The equations again identify toughness as the controlling material constant and display a conspicuous insensitivity to initial flaw size. Most important, however, is the demonstration (Figs. 3 and 4) that even small degrees of tempering can negate large increases in contact severity. Surface strengthening therefore appears to be a most attractive method for fabricating reliable, high-performance structural ceramics.

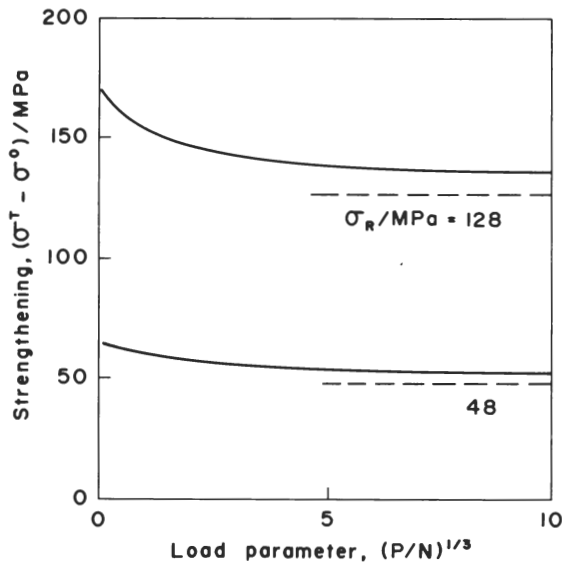


Fig. 5. Plot of strengthening function (Eq. (5)) in conjunction with Eqs. (1) and (3) at $P > P'$ for σ_R values represented in Fig. 3. Broken lines at $\sigma = \sigma_R$ are lower limits of strength.

For a given contact system, then, a strength evaluation requires only 3 specified parameters in Eq. (4), representing the specimen material (K_c), the degree of tempering (σ_R), and the indenter (χ). In the present analysis all 3 were obtained by indentation/strength calibration tests alone, with the attendant advantages indicated in Appendices A and B. This approach has special appeal for those materials in which fracture parameters are not readily measured: for K_c , a test piece suitable for direct observation of crack growth under controlled loading conditions must be made, and appropriate testing facilities must be available; for σ_R , conventional optical techniques require a transparent test material with a known stress-optical coefficient. However, where the values of these parameters are known beforehand it is possible to make reasonable *a priori* predictions of the strength degradation behavior, despite possible uncertainties (Sections III(1) and III(2)).

It is interesting to distinguish between the two main factors which contribute to the dramatic improvement in degradation resistance in tempered plates. Figure 5, representing the strengthening function of Eq. (5), is plotted in terms of indentation load in the region of indentation-controlled degradation by combination with Eqs. (1) and (3b), using parameters determined in Section III. For both tempering states represented, the contribution from the closure effect of the residual surface compression on the dominant flaw in the flexure test is shown as horizontal broken lines $\sigma^T - \sigma^0 = \sigma_R = \text{constant}$. The difference between these broken lines and the corresponding full curves is the contribution from the inhibiting effect of the residual compression on crack extension in the indentation process. For the particular indenter/specimen system represented in Fig. 5, the former effect dominates at moderate loads but the latter effect assumes gradually increasing importance as the system approaches low loads.

However satisfactory the agreement between prediction and observation may seem in the present study, the analysis involves certain assumptions which may be unjustified in other situations. Of these assumptions, those relating to the model of an ideal penny crack subjected to uniform tension (in either the indentation or the flexural field) warrant special attention. Apart from edge effects arising from the free surfaces of the plate, which may be accommodated in the fracture mechanics by a constant multiplying factor not too different from unity in the Ω parameter in Eqs. (1), (3), and (4),²³ there is the issue of stress gradients once the crack penetrates beyond the near-compression region of the plate. For thermally tempered materials, where the plate half-thickness uniquely determines the spatial scale of the stress field, gradient effects may be incorporated into the description by expanding the crack-geometry function Ω as a polynomial in c/d , for a specified

ratio σ_F/σ_R (Fig. 1), about the surface value, i.e. $\Omega = [\Omega(c/d)]_{\sigma_F/\sigma_R}$.⁸ The condition $c \ll d$ for higher-order terms to be negligible was violated in the present experiments in the extreme of high indentation loading: since $P/c^{0.3/2} = 8.2 \text{ MPam}^{1/2}$, we calculate $c^0 = 2.5 \text{ mm}$ at the upper limit $P = 1 \text{ kN}$ of the load range, which compares with the plate half-thickness $d = 1.5 \text{ mm}$. This condition causes measured strengths to deviate from predicted values, e.g. in the present tests where some of the data points in Figs. 3 and 4 corresponding to higher P values actually cross the minimum strength lines $\sigma = \sigma_R$. Although the maximum discrepancy between prediction and observation is never very much more than the scatter band in the present results, stress gradient effects are expected to play a dominant role in ultrasevere (near-failure) contact situations⁸; they are accordingly under further study in these laboratories.

Such considerations may also assume major proportions in the fracture mechanics of plates strengthened by other than thermal means; e.g. chemically tempered plates may contain residual surface stresses an order of magnitude greater than those in thermally tempered plates, but there is a similar diminution in the thickness of the compressive layer. The importance of stress gradients in the crack growth is emphasized by the analytical prediction that the chemically tempered plate is just as likely to fail catastrophically during a severe contact event.⁸ Choice of the most appropriate strengthening process for any given material therefore rests with more than merely maximizing σ_R . Practical administration of the process and maintenance of the residual field under projected in-service conditions (e.g. elevated temperatures) must also be considered.

APPENDIX A

Measurement of Residual Stress

The residual stresses in the tempered disks were measured by 2 independent techniques, in case of systematic error in the evaluation of σ_R .

(1) A conventional optical technique¹⁶ was used. A collimated polarized light beam was directed along a diameter of the disk and the stress birefringence measured with a 30-order variable compensator. The residual stress state at any point of the plate section was evaluated from the formula

$$\sigma_1 - \sigma_2 = \Delta n / A \quad (\text{A-1})$$

where σ_1 and σ_2 are the principal stresses normal to the light path, Δn is the birefringence (difference in the corresponding principal refractive indices), and A is the stress-optical coefficient. A value of A for the glass was obtained from a routine calibration test in which a known uniaxial stress was applied along a diameter of a fully annealed disk and the resultant birefringence measured for a beam of light directed along the disk axis²⁴; this procedure yielded $A = (2.84 \pm 0.1) \times 10^{-6} \text{ MPa}^{-1}$. Of the 2 principal stresses in the plate, the one parallel to the surface dominates the one normal to the surface, i.e. $\sigma_1 \gg \sigma_2$, so Eq. (A-1) effectively provides an absolute measure of the stress level.

Although in principle this technique is capable of a point-by-point determination of the entire stress profile across a disk section, in practice it is only the stress in the central plane, where gradients in the profile and interference from compositional striae are minimal, that may be measured accurately. Since it is the surface stress σ_R (not the central stress) that is pertinent to strength considerations, some assumption about the form of the stress profile must be made to extrapolate the data; for thermally tempered plate a parabolic profile is generally a good approximation, in which case the magnitude of the surface compressive stress is ideally twice that of the central tensile stress.⁹ Uncertainties also arise because the birefringence is averaged over the optical path length; σ_R may be subject to considerable systematic variation across the diameter of a tempered disk.²⁵

(2) Residual stresses were measured by the indentation tests themselves.¹³ In this technique tempered and untempered (control) surfaces are indented at a prescribed load and comparative measurements from the ensuing crack patterns are used to evaluate the stresses in the tempered plate. This is quantified from Eq. (1)

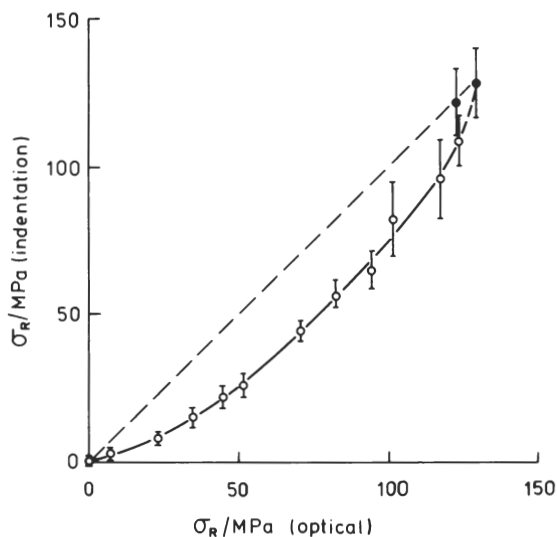


Fig. A-1. Comparative plot of surface residual stress in thermally tempered glass lenses, as measured by indentation and optical techniques; each data point represents a single lens. Vertical error bars are standard deviations for ≥ 10 indentations; reproducibility of optical measurements is better than 1 MPa. Filled symbols represent as-received tempered specimens, open symbols partially annealed tempered specimens; broken line represents $\sigma_R(\text{indentation}) = \sigma_R(\text{optical})$.

$$\sigma_R = [K_c / (\pi \Omega c^T)^{1/2}] \{ (c^0 / c^T)^{3/2} - 1 \} \quad (P \text{ constant}) \quad (\text{A-2})$$

where c^0 and c^T are crack sizes at the same load. In the present tests a load $P = 100$ N produced sufficiently well-developed indentation patterns to allow crack dimensions to be measured from surface traces¹³; K_c was taken from the indentation/strength tests on fully annealed disks (see Section III(2)) and the small-scale fracture approximation $\Omega \approx 4/\pi^2$ was retained. This indentation method provides a direct measure of the stress term σ_R at any given point on the disk surface.

Optical and indentation measurements of σ_R for tempered glass disks are compared in Fig. A-1. Approximately equal values are obtained from the 2 techniques for as-received disks in their fully tempered state, but for disks which have subsequently been subjected to annealing the optical value is systematically greater than the indentation value. This discrepancy is attributed to the extrapolation procedure used to evaluate the surface compressive stress in the optical tests. The annealing of glass involves many complex stress relaxation processes, and regions of higher stress level relax much more rapidly than would be predicted from a simple thermal activation process.²⁶ Thus the stress profile in a thermally tempered plate will anneal more rapidly near the outer surfaces, so that any extrapolated estimate of σ_R will overestimate the true value. The indentation technique is not susceptible to this type of systematic error, and, in spite of a considerably greater scatter in the data (see error bars in Fig. A-1), is preferred in the present analysis.

APPENDIX B

Measurement of Critical Stress-Intensity Factor

For the glass used in the present study the value of K_c obtained by the indentation/strength procedure of Section III(2) was $\approx 40\%$ lower than that obtained independently by the more direct double-cantilever technique. Similar discrepancies have been reported by Petrovic *et al.*²¹ with SiC and Si₃N₄. These writers suggested that residual stresses due to the deformation processes about the hardness-impression (giving rise to mismatch strains at the interface between plastic zone and surrounding elastic matrix²⁷) enhance the driving force for indentation fracture, thereby giving a depressed value of K_c from indentation/strength measurements. They tested a series of specimens in which the hardness impression was progressively rendered ineffective as a source of residual stress (either by grinding away the surface or annealing, between indentation and

strength testing), and showed that the discrepancy correspondingly diminished.

The significance of residual stress effects for the present experiments was checked by the optical technique (Appendix A). Indentations in a fully annealed disk were examined normal to the plate surface between crossed polars and the indentation birefringence was measured with the compensator. For a Vickers indentation produced at a load of 100 N (impression half-diagonal $a = 94$ μm for the deformation and surface trace half-length $c^0 = 502$ μm for the fracture) the maximum optical retardation (located close to the sides of the impression) was ≈ 200 nm. If the path length over which the retardation is produced is approximately equal to the depth of the deformation zone responsible for the residual stress, viz. $\approx a = 94$ μm , then an average birefringence $\Delta n \approx 2.1 \times 10^{-3}$ is obtained; from Eq. (A-1), the corresponding residual stress is $\sigma_r \approx \sigma_1 - \sigma_2 \approx 750$ MPa. In terms of an equivalent driving force for the crack,²² multiplying σ_r by the cross-sectional area of the deformation zone over which it acts, viz. $\approx a^2 = 8.8 \times 10^3$ μm^2 , gives $P_{r,\perp} \approx 6.6$ N acting perpendicular to the median plane of the indentation; the stress-intensity factor for a median half-penny crack center-loaded with such a perpendicular force (the assumption of center-loading remaining valid for $c^0 \gg a$) follows from the standard formula⁵ $K_r = 2P_{r,\perp} / (\pi c^0)^{3/2}$ (note this is a special case of Eq. (1a)) ≈ 0.21 MPa. This value of K_r is of the same order as the discrepancy in K_c values noted earlier.

Any experimental determination of the stress-intensity factor for cracks produced by a sharp indenter must therefore be expected to contain a component due to local residual stresses, so that the apparent value

$$K_c' = K_c - K_r \quad (\text{B-1})$$

at equilibrium should be regarded as an *effective* rather than *true* stress-intensity factor. Accordingly, it is K_c' and not K_c which should appear in the formulation of Eqs. (1), (2), (4), (5), and (7) relating to the extension of indentation cracks. The (apparent) stress-intensity factor obtained directly from the indentation/strength calibration tests on untempered control specimens is thus the appropriate value to use in the degradation analysis.

Acknowledgment: The writers are grateful to S. M. Wiederhorn for carrying out the independent K_c measurements on the glass plates.

References

- B. R. Lawn and T. R. Wilshaw, "Indentation Fracture: Principles and Applications," *J. Mater. Sci.*, **10** [6] 1049–81 (1975).
- B. R. Lawn, S. M. Wiederhorn, and H. H. Johnson, "Strength Degradation of Brittle Surfaces: Blunt Indenters," *J. Am. Ceram. Soc.*, **58** [9–10] 428–32 (1975).
- B. R. Lawn, E. R. Fuller, and S. M. Wiederhorn, "Strength Degradation of Brittle Surfaces: Sharp Indenters," *ibid.*, **59** [5–6] 193–97 (1976).
- S. M. Wiederhorn and B. R. Lawn, "Strength Degradation of Glass Resulting from Impact with Spheres," *ibid.*, **60** [9–10] 451–58 (1977).
- B. R. Lawn and E. R. Fuller, "Equilibrium Penny-Like Cracks in Indentation Fracture," *J. Mater. Sci.*, **10** [12] 2016–24 (1975).
- F. M. Emsberger, "Strength of Brittle Ceramic Materials," *Am. Ceram. Soc. Bull.*, **52** [3] 240–46 (1973).
- (a) H. P. Kirchner, R. E. Walker, and D. R. Platts, "Strengthening Alumina by Quenching in Various Media," *J. Appl. Phys.*, **42** [10] 3685–92 (1971).
- (b) R. M. Gruver and H. P. Kirchner, "Effect of Surface Damage on the Strength of Al₂O₃ Ceramics with Compressive Surface Stresses," *J. Am. Ceram. Soc.*, **56** [1] 21–24 (1973).
- B. R. Lawn and D. B. Marshall, "Contact Fracture Resistance of Physically and Chemically Tempered Glass Plates: A Theoretical Model," *Phys. Chem. Glasses*, **18** [1] 7–18 (1977).
- J. T. Littleton and F. W. Preston, "A Theory of the Strength of Thermally Toughened Glass," *J. Soc. Glass Technol.*, **13** [52] 336–49 (1929).
- F. P. Mallinder and B. A. Proctor, "Elastic Constants of Fused Silica as a Function of Large Tensile Strain," *Phys. Chem. Glasses*, **5** [4] 91–103 (1964).
- B. R. Lawn and T. R. Wilshaw, *Fracture of Brittle Solids*; Ch. 3. Cambridge University Press, London and New York, 1975.
- M. Prod'homme, "Some Results Concerning the Microhardness of Glasses," *Phys. Chem. Glasses*, **9** [3] 101–105 (1968).
- D. B. Marshall and B. R. Lawn, "An Indentation Technique for Measuring Stresses in Tempered Glass Surfaces," *J. Am. Ceram. Soc.*, **60** [1–2] 86–87 (1977).
- A. G. Evans and R. W. Davidge, "A Biaxial Stress Method for the Determination of the Strength of Sections Cut from Glass Containers and the Size of the Critical Griffith Flaws," *Glass Technol.*, **12** [6] 148–54 (1971).
- D. B. Marshall and B. R. Lawn, "Measurement of Surface Stresses from Indentation Microfractures"; in Seventh Australian Ceramic Conference Proceedings. Australian Ceramic Society, Sydney, 1976.
- A. J. Monack and E. E. Beeton, "Analysis of Strains and Stress in Glass: I," *Glass Ind.*, **20** [4] 127–32 (1939); "II," *ibid.*, [5] 185–91; "III," *ibid.*, [6] 223–28; "IV," *ibid.*, [7] 257–62.
- N. Shinkai, K. Okami, S. Miyoshi, and K. Akeyoshi, "Indentation Fracture of Tempered Glasses," *Asahi Garasu Kenkyu Hokoku*, **23** [2] 83–99 (1973).
- T. R. Wilshaw, "Measurement of Tensile Strength of Ceramics," *J. Am. Ceram. Soc.*, **51** [2] 111 (1968).

- ¹⁹ B. R. Lawn, T. Jensen, and A. Arora, "Brittleness as an Indentation Size Effect," *J. Mater. Sci.*, **11** [3] 573-75 (1976).
- ²⁰ S. M. Wiederhorn, "Fracture Surface Energy of Glass," *J. Am. Ceram. Soc.*, **52** [2] 99-105 (1969).
- ²¹ J. J. Petrovic, R. A. Dirks, L. A. Jacobson, and M. G. Mendiratta, "Effects of Residual Stresses on Fracture from Controlled Surface Flaws," *ibid.*, **59** [3-4] 177-78 (1976).
- ²² M. V. Swain, "A Note on the Residual Stress About a Pointed Indentation Impression in a Brittle Solid," *J. Mater. Sci.*, **11** [12] 2345-48 (1976).

- ²³ A. S. Kobayashi; pp. 4-37 in *Experimental Techniques in Fracture Mechanics*. Edited by A. S. Kobayashi. Iowa State University Press, Ames, Ia., 1973.
- ²⁴ J. W. Dally and W. F. Riley, *Experimental Stress Analysis*; Ch. 8. McGraw-Hill, New York, 1965.
- ²⁵ D. B. Marshall and B. R. Lawn, "Non-Uniform Distribution of Residual Stresses in Tempered Glass Disks"; to be published in *Glass Technology*.
- ²⁶ G. O. Jones, *Glass*, 2d ed.; Ch. 5. Chapman and Hall, London, 1972.
- ²⁷ B. R. Lawn, M. V. Swain, and K. Phillips, "Mode of Chipping Fracture in Brittle Solids," *J. Mater. Sci.*, **10** [7] 1236-39 (1975).